American Mineralogist, Volume 64, pages 809–823, 1979

The stability field of anthophyllite: the effect of experimental uncertainty on permissible phase diagram topologies

HOWARD W. DAY

Department of Geology, University of California
Davis, California 95616

AND HEINER HALBACH

Institut für Mineralogie, Ruhr Universität-Bochum
D 4630 Bochum, Federal Republic of Germany

Abstract

We have examined experimental data for reactions among anthophyllite, enstatite, forsterite, quartz, talc, and water, using linear programming methods, in order to examine the range of internally consistent thermodynamic data sets that is permitted by the experiments. Phase diagrams calculated using the derived thermodynamic parameters may have all topologies previously proposed to describe the anthophyllite stability field as well as others. Depending upon the experimental data analyzed, phase diagrams in close agreement with calorimetrically measured thermodynamic parameters may have the topology originally proposed by Greenwood (1963) or the topology he sketched (Greenwood, 1971) in revising his original ideas. The experimental data of Chernosky (1976) and Greenwood (1963) appear not to be consistent with the available calorimetric data for the above minerals within their stated uncertainties. This discrepancy is most easily explained if there exists a major difference between the properties of talcs used in the experiments and that used for calorimetric measurements or if the calorimetric measurements are incorrect. A similar difference in the properties of anthophyllite may also be indicated.

Introduction

Greenwood (1963) demonstrated for the first time that the orthorhombic amphibole, anthophyllite, has an extensive stability field in the system magnesia–silica–water. Using thermodynamic data and the results of his experiments, he suggested that the stability of anthophyllite was limited at both low and high temperatures by dehydration reactions and that the stability field terminated at about twenty kbar by the anhydrous decomposition of anthophyllite to enstatite plus talc (Fig. 1).

Chernosky (1976) and Hemley *et al.* (1977a, b) have made new experiments in the system magnesia–silica–water. Chernosky (1976) combined his data with experiments by Skippen (1971) and Greenwood (1963), and favored the topology illustrated by Greenwood (1963); he suggested, however, that the anthophyllite field might terminate at pressures as low as five kbar. Chernosky recognized some apparent inconsistencies between his experiments and Greenwood's, and suggested that a phase diagram topology in which anthophyllite stability terminated at low pressures might be required in order to resolve these discrepancies. Hemley *et al.* (1977a, b) reported equilibrium temperatures at one kbar for several reactions in the system magnesia–silica–water. They calculated a phase diagram using these temperatures and thermodynamic data, some of which were derived from the experiments. This diagram, Figure 2, appears to contradict that favored by Chernosky (1976) and Greenwood (1963).

Chernosky and Knapp (1977) have reported additional experiments and have concluded that the anthophyllite field is best described by the phase diagram proposed by Hemley *et al.* (1977b).

Any attempt to decide between alternatives should proceed with a clear idea of the uncertainties involved. Toward this end, we have investigated the possible thermodynamically consistent phase dia-

0003–004X/79/0708–0809$02.00

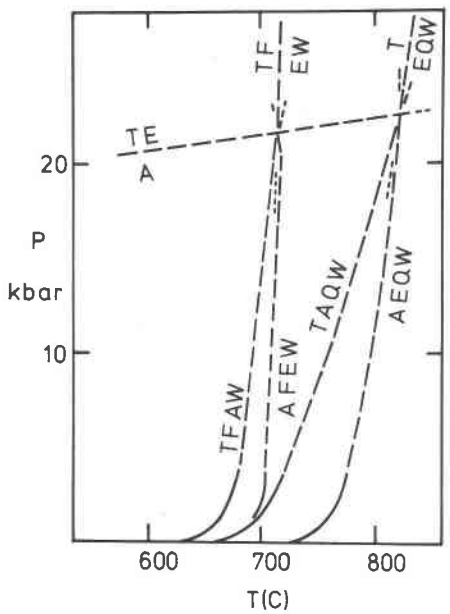

Fig. 1. Topology of equilibria in the system $MgO–SiO_2–H_2O$ proposed by Greenwood (1963).

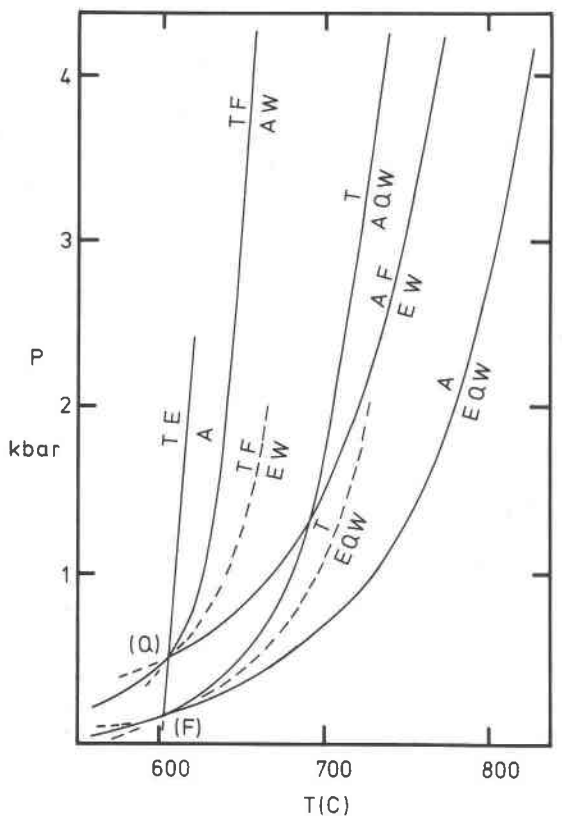

Fig. 2. Topology of equilibria in the system $MgO–SiO_2–H_2O$ proposed by Hemley *et al.* (1977b).

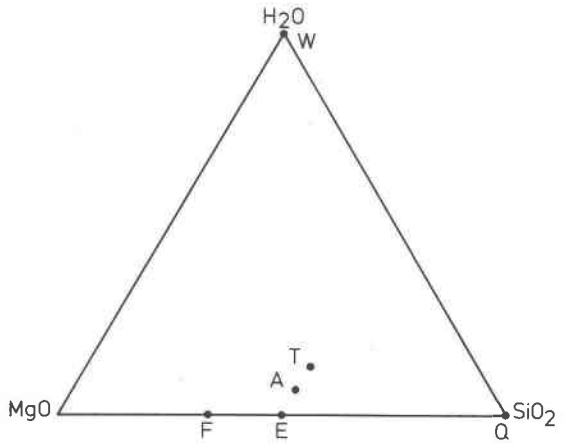

Fig. 3. Molar composition of minerals in the system $MgO–SiO_2–H_2O$.

grams that satisfy the experimental data. Using linear programming methods (Gordon, 1973; Day and Kumin, 1977, 1979; Halbach and Chatterjee, 1978), we have derived limiting sets of internally consistent thermodynamic parameters from the experiments and have used these parameters to calculate thermodynamically consistent phase diagrams that pass through all experimental brackets from which the parameters were derived. We have made a special effort to separate consideration of what the experimental data by themselves permit from the possible further constraints of calorimetric data on permissible phase diagrams. We emphasize an analysis of experiments reported by Chernosky (1976) and Chernosky and Knapp (1977), because these data place more critical constraints on the possible phase diagrams, independent of other thermodynamic assumptions, than either the experiments of Hemley *et al.* (1977a,b) or Greenwood (1963).

We will show that several phase diagram topologies are permitted by the experiments, but the one that seems to fit the experimental data best has a topology first suggested by Greenwood (1971). On the other hand, the best agreement with calorimetric data is found when the phase diagram has a topology similar to that proposed by Greenwood (1963).

The phases with which we are concerned are illustrated in Figure 3, and some of their properties are documented in Table 1. The equilibria are listed in Table 2 along with equations of linear dependence by which these reactions are related.

Methods of thermodynamic analysis

The approach we have followed is based on the extensive discussions of Chatterjee (1970, 1977), Fisher

Table 1. Composition and properties of substances in the system magnesia–silica–water

PHASE		COMPOSITION	VOLUME[1] (cm^3)	HEAT CAPACITY COEFFICIENTS[2] A	B	C	H°_F (J)	S°_F (J/K)
Anthophyllite	(A)	$Mg_7Si_8O_{22}(OH)_2$	264.46	842.513	163.121	-221.502	-12083059[3]	
				(821.403)	(182.088)	(-196.481)	± 8088	
Enstatite	(E)	$MgSiO_3$	31.47	102.717	19.832	- 26.276		-291.139[4]
								± 2.449
Forsterite	(F)	Mg_2SiO_4	43.79	149.829	27.363	- 35.648	- 2170166[6]	-398.995[5]
							± 1918	± 0.882
α Quartz	(Q)	SiO_2	22.688	46.944	34.309	- 11.297	- 910648[5]	-182.489[5]
							± 1674	± 0.125
β Quartz				60.291	8.117			
Talc	(T)	$Mg_3Si_4O_{10}(OH)_2$	136.25	414.470	100.126	-109.370	-5916200[7]	-1273.082[5]
							± 7200	± 0.844
Hydrogen		H_2		27.280	3.264	- 0.502		
Oxygen		O_2		29.957	4.184	- 1.674		

[1]Formula unit volumes are taken from Robie and Waldbaum (1968) except for anthophyllite, which was given by Greenwood, (1963). The value for enstatite is for the monoclinic form.

[2]Most Heat capacities have been recalculated from Kelley (1960). Values for talc and anthophyllite are discussed in the text. Values in parentheses are calculated from Table 3, Hemley and others (1977b). $Cp = A + B\ (10^{-3})\ T + C\ (10^5)\ T^{-2}$ (J/K).

[3]Weeks (1956). Includes a correction of about 47 kJ for the iron content of the amphibole. We made an additional correction of about 4.5 kJ for the calcium content, assuming it was present as tremolite.

[4]This entropy is for clinoenstatite. Zen and Chernosky (1976) have argued that the entropy of orthoenstatite is not much different. We have arbitrarily increased the uncertainty by 2 J/°K in order to estimate permissable limits on the entropy of formation of orthoenstatite.

[5]Robie and Waldbam, 1968.

[6]Based on unpublished value of G°_f by Hemingway and Robie, as reported by Zen and Chernosky, 1976, and the entropy listed above.

[7]Zen and Chernosky (1976) based on data originally reported by Barany, 1963.

and Zen (1971), and Zen (1969, 1972). These authors have shown that the equilibrium conditions for a dehydration reaction may be written (see Table 3 for a summary of notation)

$$\Delta G_r(T,P) = \Delta H_{fs}^\circ(298,1) - T\Delta S_{fs}^\circ(298,1) + G'(T,P) \quad (1)$$

where the last term is

$$G'(T,P) = \int_{298}^{T} \Delta Cp_{fs}\,dT - T\int_{298}^{T} \Delta Cp_{fs}/T\,dT + \Delta V_s(P-1) + n_w G_w^*(T,P) \quad (2)$$

This statement of the equilibrium condition ignores the possible effects of thermal expansion and compressibility on the solids but is otherwise exact.

If the volumes and heat capacities of the solid phases are known, these data may be combined with the properties of water (Fisher and Zen, 1971) in order to calculate the value of $G'(T,P)$ at the temperature and pressure of any experiment and to place limits on the enthalpy and entropy of the reaction. Most hydrothermal experiments lie in the stability field of either the products or the reactants. In the first case, $\Delta G_r(T,P) \leq 0$, and in the second, $\Delta G_r(T,P) \geq 0$. Therefore, if the products are stable in an experiment,

$$-\Delta H_{fs}(298,1) + T\Delta S_{fs}(298,1) \geq G'(T,P) \quad (3)$$

Table 2. Reactions and equations of linear dependence in the system magnesia–silica–water

R1.	(TEQW)	T = 3 E + Q + W	R5 + 3 R4 - 7 R1 = 0
R2.	(TFEW)	T + F = 5 E + W	R4 + R7 - R1 = 0
R3.	(AFEW)	A + F = 9 E + W	R2 - R3 - R7 = 0
R4.	(AEQW)	A = 7 E + Q + W	9 R2 - R6 - 5 R3 = 0
R5.	(TAQW)	7 T = 3 A + 4 Q + 4 W	R4 - R3 - R9 = 0
R6.	(TFAW)	9 T + 4 F = 5 A + 4 W	9 R4 - 7 R3 - R10 = 0
R7.	(TEA)	T + 4 E = A	2 R6 + 5 R10 - 9 R8 = 0
R8.	(TFQW)	2 T = 3 F + 5 Q + 2 W	R10 - 2 R11 - R8 = 0
R9.	(EFQ)	2 E = F + Q	
R10.	(AFQW)	2 A = 7 F + 9 Q + 2 W	
R11.	(AFTQ)	A = 2 F + T + 2 Q	

Table 3. Thermodynamic notation

T,P	Temperature (K), Pressure (bars)
H°_f	Standard state enthalpy of formation from the elements (J/gfw)
S°_f	Standard state entropy of formation from the elements (J/K-gfw)
C_{pf}	Heat capacity of formation from the elements (J/K-gfw)
G^*_w	$G^\circ_{f,\ H_2O}(T,1) + G_{H_2O}(T,P) - G_{H_2O}(T,1)$ (Fisher and Zen, 1971)
r	subscript indicating "of reaction".
s	subscript indicating "due to solids in reactions".

and if the reactants are stable, the inequality must be reversed. All values of delta H and delta S satisfying such an inequality lie in a closed half-space in an enthalpy–entropy graph. If at least three such inequalities are available, it is possible to describe a bounded portion of enthalpy–entropy space that contains all thermodynamic data sets satisfying the experiments.

The permissible solutions for the enthalpy and entropy of the solids in reaction TEQW (Table 2) are illustrated in Figure 4. The thermodynamic parameters that satisfy the four limiting TEQW experiments (nos. 1, 2, 5, and 8, Table 4) are restricted to the shaded region known as a feasible solution space. The calculation procedures will be discussed in more detail at a later point in the paper. For now it is only important to note that vertices *a* and *b* in Figure 4 define the maximum and minimum permissible values of enthalpy and entropy that are consistent with the experiments. However, these vertices do not describe particularly useful uncertainty ranges, because the values of enthalpy and entropy may not be combined independently but must lie only in the narrow feasible solution space. Because any combination of enthalpy and entropy along line 8 (Fig. 4) may be used to calculate a P–T curve passing through limiting experiment 8, a phase diagram calculated using the coordinates of vertex *a* would pass through both limiting experiments 1 and 8. Likewise a diagram calculated using the coordinates of vertex *b* would pass through experiments 2 and 5. Coordinates inside the feasible solution space could be used to calculate an equilibrium curve that passes between all experimental brackets without intersecting a limiting experiment.

Gordon (1973) pointed out that the concept of a feasible solution space is easily extended to accommodate problems involving several reactions, and that it is possible to find coordinates in such multidimensional feasible solution spaces using the techniques of linear programming. Gordon (1973), Day and Kumin (1977, 1979), and Halbach and Chatterjee (1978) have outlined the use of this technique for thermodynamic problems. Briefly, linear programming is a procedure by which a set of linear constraints such as equation 3 may be analyzed to find an optimal solution according to an objective criterion. For our problem this means: find a set of thermodynamic variables that maximizes or minimizes a linear combination of these parameters. In the general case, a different optimal solution may be found for each possible choice of the objective function.

In order to analyze the feasible solution space in Figure 4, one might choose the objective criteria (where Z is known as an "objective function"):

$$\text{maximize } Z = \Delta H_{fs}(298,1)$$

or

$$\text{minimize } Z = \Delta S_{fs}(298,1)$$

In the first case, the linear programming algorithm would locate the coordinates of vertex *b*, and in the second, the coordinates of vertex *a*. The other two vertices could be located by maximizing and mini-

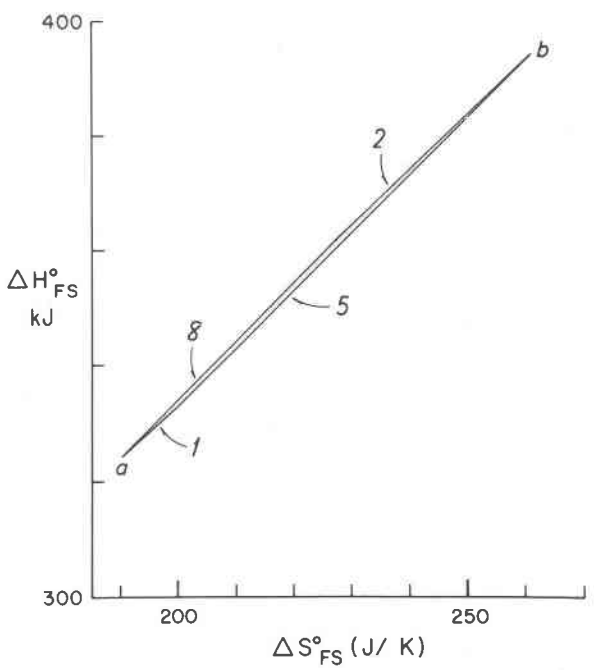

Fig. 4. The feasible solution space for the enthalpy and entropy of the reaction T = E + Q + W. The experiments on which these calculations are based are discussed in the text and listed in Table 4.

mizing an objective function having a slope between those of lines 2 and 8 and between those of lines 1 and 5:

$$Z = \Delta H_{fs}(298,1) + 980\,\Delta S_{fs}(298,1)$$

Important advantages of the linear programming approach are, first, that the entire range of permissible thermodynamic parameters is accessible for inspection by the appropriate choice of objective criteria; second, that any constraint on the thermodynamic variable, such as calorimetric data, that may be written as a linear combination of the variables may be added to the problem; third, that the constraints provided by experiments may be examined independently of additional thermodynamic assumptions or *with* such additional assumptions, depending on the goals of the investigation; fourth, that no solution obtained can violate any experimental or thermodynamic constraint in the data set.

Data and calculation procedures

The eleven possible balanced reactions among water and the five solid phases listed in Table 1 are given in Table 2. Since there are three independent reactions, the equations describing the linear dependence of the eleven reactions (Table 2) may be used to derive all other reactions from any group of three known reactions, provided that the three also contain all six phases. The enthalpies and entropies of the eleven reactions are also related in the same way, so that eight pairs of similar equations place limits on the permissible reaction enthalpies and entropies. These have been mentioned by Gordon (1973) as "theoretical constraints" and must be added to any analysis that is written in terms of the reaction properties.

For our initial analysis we used the hydrothermal experiments reported by Chernosky (1976) and Chernosky and Knapp (1977), with one additional pair of experiments from Skippen (1971). The properties of the synthetic phases have been documented by these authors, but it is useful to note that TEM investigations show the anthophyllites used in these experiments to be disordered with respect to silicate chain width (Chernosky, 1978, personal communication). The experiments include two or more sets of brackets on four of the reactions in Table 2: R1, R2, R4, and R5. Since all six phases of interest are included in these four reactions, thermodynamic parameters derived from this set of experiments may be used to calculate the enthalpies and entropies of the other seven reactions independently of additional assumptions about the properties of the participating phases.

Table 4. Experimental constraints on the thermodynamic properties of reactions R1, R2, R4, and R5 calculated from Chernosky (1976), Chernosky and Knapp (1977), and Skippen (1971). GE and LE mean "greater than or equal to" and "less than or equal to" respectively.

	Experimental T and P				Constraint on enthalpy and entropy of reaction					
	nominal °C	nominal bars	expanded °C	expanded bars	T(K)				Joules	
					R1: T = 3 E + Q + W					
1.	648	500	643	510	− ΔH(1)	+	916.15	ΔS(1)	LE	−149502.066
2.	672	500	677	490	− ΔH(1)	+	950.15	ΔS(1)	GE	−145582.273
3.	684	867	679	884	− ΔH(1)	+	952.15	ΔS(1)	LE	−142364.927
4.	718	1200	723	1176	− ΔH(1)	+	996.15	ΔS(1)	GE	−135271.112
5.	729	1800	724	1836	− ΔH(1)	+	997.15	ΔS(1)	LE	−133304.650
6.	744	2000	749	1960	− ΔH(1)	+	1022.15	ΔS(1)	GE	−129506.475
7.	726	2000	721	2040	− ΔH(1)	+	994.15	ΔS(1)	LE	−133338.448
8.	740	2000	745	1960	− ΔH(1)	+	1018.15	ΔS(1)	GE	−130075.011
					R2: T + F = 5 E + W					
1.	600	500	595	510	− ΔH(2)	+	868.15	ΔS(2)	LE	−153859.748
2.	621	500	626	490	− ΔH(2)	+	899.15	ΔS(2)	GE	−150032.677
3.	637	1000	632	1020	− ΔH(2)	+	905.15	ΔS(2)	LE	−146425.750
4.	657	1000	652	980	− ΔH(2)	+	925.15	ΔS(2)	GE	−143743.821
5.	640	2000	635	2040	− ΔH(2)	+	908.15	ΔS(2)	LE	−144326.991
6.	663	2000	668	1960	− ΔH(2)	+	941.15	ΔS(2)	GE	−139474.104
7.	662	3000	657	3060	− ΔH(2)	+	930.15	ΔS(2)	LE	−140286.918
8.	692	3000	697	2940	− ΔH(2)	+	970.15	ΔS(2)	GE	−134191.658
9.	686	4000	681	4080	− ΔH(2)	+	954.15	ΔS(2)	LE	−136171.632
10.	706	4000	711	3920	− ΔH(2)	+	984.15	ΔS(2)	GE	−131510.961
					R4: A = 7 E + Q + W					
1.	673	500	668	510	− ΔH(4)	+	941.15	ΔS(4)	LE	−144146.096
2.	687	500	692	490	− ΔH(4)	+	965.15	ΔS(4)	GE	−141309.174
3.	719	1000	714	1020	− ΔH(4)	+	987.15	ΔS(4)	LE	−134668.035
4.	729	1000	734	980	− ΔH(4)	+	1007.15	ΔS(4)	GE	−132083.722
5.	748	1500	743	1530	− ΔH(4)	+	1016.15	ΔS(4)	LE	−128886.582
6.	754	1500	759	1470	− ΔH(4)	+	1032.15	ΔS(4)	GE	−126742.829
7.	772	2000	767	2040	− ΔH(4)	+	1040.15	ΔS(4)	LE	−124262.539
8.	778	2000	783	1960	− ΔH(4)	+	1056.15	ΔS(4)	GE	−122046.712
					R5: 7 T = 3 A + 4 Q + 4 W					
1.	645	500	640	510	− ΔH(5)	+	913.15	ΔS(5)	LE	−605913.143
2.	699	500	674	490	− ΔH(5)	+	947.15	ΔS(5)	GE	−590821.837
3.	690	1500	685	1530	− ΔH(5)	+	958.15	ΔS(5)	LE	−564214.430
4.	700	1500	705	1470	− ΔH(5)	+	978.15	ΔS(5)	GE	−554109.497
5.	702	2000	697	2040	− ΔH(5)	+	970.15	ΔS(5)	LE	−553376.210
6.	712	2000	717	1960	− ΔH(5)	+	990.15	ΔS(5)	GE	−542954.324
7.	720	3000	715	3060	− ΔH(5)	+	988.15	ΔS(5)	LE	−537272.066
8.	740	3000	745	2940	− ΔH(5)	+	1018.15	ΔS(5)	GE	−520761.649

Chernosky (1976) estimated that his reported temperatures and pressures are accurate to within 5°C and 2 percent of the reported pressure. In order to provide more realistic estimates of the outside limits on the location of equilibrium curves and in order to promote interlaboratory comparisons, we have expanded all experimental brackets by these amounts in opposite directions away from the location of the equilibrium curves (Table 4). Values of $G'(T,P)$ were calculated at each modified temperature and pressure, using the data and procedures discussed below. The 34 experimental temperatures and pressures are listed in Table 4 along with the values of G' and the

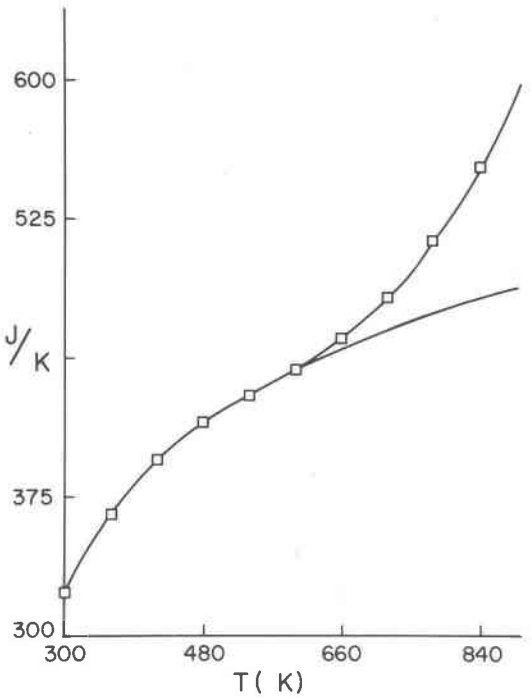

Fig. 5. Heat capacity of talc as a function of temperature. The upper curve represents the equation reported by Krupka *et al.* (1977). The lower curve is the Maier–Kelley type equation we have used.

implied constraints on the thermodynamic properties of the reactions.

The molar volumes and high-temperature heat capacities needed to calculate values of G' for each experiment are listed in Table 1. The molar volumes were taken from the references listed in the table. Most of the heat capacities have been recalculated from Kelley (1960), but the values for talc and anthophyllite deserve special comment.

Krupka *et al.* (1977) have made new heat-capacity determinations for talc and have reported their results for the interval 298.15 K–650 K in the form: $Cp = a + bT + cT^{-2} + dT^{-2} + eT^{-1/2}$. Equations of this form may cause a rapid increase in apparent heat capacity immediately above the highest temperature for which data are available, as shown in Figure 5. Consequently, we have expressed their results as a Maier–Kelley type equation according to the following procedure.

Because we are primarily interested in the integrals of the heat capacity function (see equation 1), we made a least-squares regression on values of

$$\int_{298}^{T} Cp\, dT$$

calculated from the equation reported by Krupka *et al.* Unfortunately, the data on which their equation is based have not yet been published. In order to provide a better extrapolation above the maximum reported temperature, we weighted the regression arbitrarily by calculating the integral at 12 equally-spaced temperatures in the upper half of the reported interval and at nine equally-spaced temperatures (including 298.15 and the mid-point) in the lower half of the reported interval. Our least-squares fit to these 21 points is reported as a Maier–Kelley function of the heat capacity in Table 1. Although the weighting scheme we have used is arbitrary, a different scheme would not affect our conclusions.

Zen and Chernosky (1976) have pointed out that the properties of anthophyllite are poorly known. White (1919) reported six measurements of the gram-specific heat content at temperatures up to 1160°C for a material characterized only as "Mag. Sil., Amphibole." Goranson (in Birch *et al.*, 1942, p. 230) and Kelley (1960) have reported Maier–Kelley type heat capacity functions that fit these six measurements. Goranson's function is reported as Joules per gram and Kelley's as calories per 100.41 grams (the formula weight for $MgSiO_3$). Either function may be used to calculate comparable values for the heat capacity of one formula weight of anthophyllite (780.874 grams).

The high-temperature entropies used by Zen and Chernosky (1976) in their analysis of the equilibria in Table 2 were calculated from the experimental data of Greenwood (1963) by Mel'nik and Onoprienko (1969), using the heat capacity function of Goranson. Hemley *et al.* (1977b) have used an approximate heat capacity function that is eight times that reported by Kelley (1960), implying a formula weight for anthophyllite of 803.28 grams. Because the analyzed material was so poorly characterized, Hemley *et al.* simply rounded the formula weight ratio, anthophyllite/enstatite, to eight to derive the approximate heat capacity (Hemley, 1978, personal communication).

Since the studies by Zen and Chernosky (1976) and Hemley *et al.* (1977b), new measurements of the heat capacity of tremolite have been reported (Krupka *et al.*, 1977) that permit a new estimate of the heat capacity of anthophyllite. Because of the uncertainties concerning the procedures and material used by White (1919), we prefer to use the estimated heat capacity until new measurements are reported. The heat capacity of anthophyllite was estimated ac-

cording to the scheme:

$$Cp[Mg_7Si_8O_{22}(OH)_2]$$
$$= Cp\,[Ca_2Mg_5Si_8O_{22}(OH)_2]$$
$$+ 4\,Cp\,(MgSiO_3)$$
$$- 2\,Cp\,(CaMgSi_2O_6)$$

The heat capacity function for tremolite (A = 874.061, B = 149.397, C = −248.112) was derived from the equation reported by Krupka *et al.*, using the procedure discussed previously for talc. The heat capacity functions for clinoenstatite and diopside were taken from Kelley (1960). The resulting heat capacity function for anthophyllite is listed in Table 1. The estimated function produces heat capacities that are between 10–30 J/°K (2–4%) more positive than those based on the measurements of White, and are fortuitously very similar to those based on the approximate function used by Hemley *et al.* (1977b).

The values of $G'(T,P)$ (equation 2) were calculated for each experimentally-determined pressure and temperature, using a computer program (GPRIM1) written in FORTRAN (Day, unpublished). The thermodynamic effects of the alpha–beta quartz transition are taken into account by using the heat capacity functions appropriate for the interval being integrated and by using the known entropy of the alpha–beta transition (1.42256 J = 0.34 cal; Robie and Waldbaum, 1968). The values of $G^{\circ}_{w}(T,P)$ (Fisher and Zen, 1971) were computed using the subroutines FFIND and GH20 (Holloway *et al.*, 1971), which are based on the properties of water measured by Burnham *et al.* (1969). The calculated values of $G^{\circ}_{w}(T,P)$ agree well with those reported by Fisher and Zen (1971) except in P–T regions near the limits of the polynomial functions used in the subroutines.

The 34 experiments in Table 4 combined with eight pairs of linear dependence equations (Table 2) are sufficient to describe the feasible solution space containing all combinations of enthalpy and entropy of reaction that are compatible with the experimental data. This feasible solution space has 22 dimensions corresponding to the enthalpies and entropies of the 11 reactions. Any point in this feasible solution space is defined by 22 coordinates, and each such point corresponds to an internally-consistent set of thermodynamic parameters that satisfies the experimental brackets. The only thermodynamic assumptions implicit in any such feasible solution are those required to calculate the values of $G'(T,P)$ (equation 2).

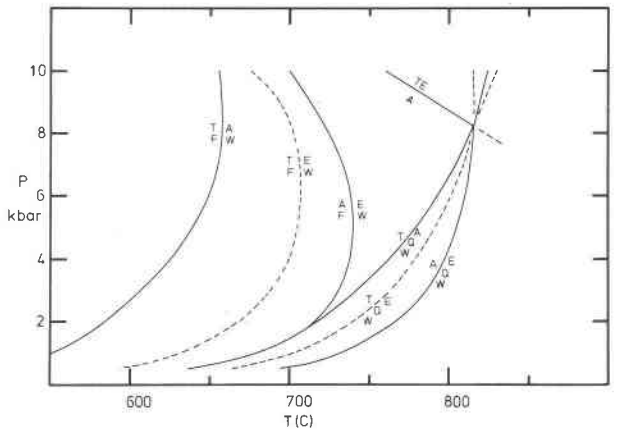

Fig. 6. Phase diagram having the minimum possible entropy of reaction TFAW.

We have examined some limiting sets of thermodynamic parameters from this feasible solution space in order to investigate the range of permissible phase diagrams. For each of the eleven reactions in Table 2, we defined two objective criteria:

$$\text{maximize } Z = \Delta S_{fs}(298,1)$$

and

$$\text{minimize } Z = \Delta S_{fs}(298,1)$$

These objective criteria were used to locate a feasible solution, using a linear programming routine developed and written by H. Halbach. Details of this algorithm will appear as part of his doctoral dissertation at Ruhr Universität-Bochum, but the results were found to be compatible with those reached using other systems available in most computing centers. Some of the 22 objective criteria defined above are satisfied at the same point in the feasible solution space, so that we found only 12 unique sets of thermodynamic parameters in this fashion.

Each set of thermodynamic data was used to calculate a complete phase diagram from 100 bars to 10 kbar, using a computer program (TEQ) written in FORTRAN (Day, unpublished). This program uses the same thermodynamic information as program GPRIM1 and the values of $\Delta H_{fs}(298,1)$ and $\Delta S_{fs}(298,1)$ to calculate the equilibrium temperature of a reaction at a specified pressure. The computation is done by an iterative procedure that continues to test possible equilibrium temperatures until one is found for which the free energy of the reaction is less than ±1 Joule. Output is a list of equilibrium temperatures for the specified pressures.

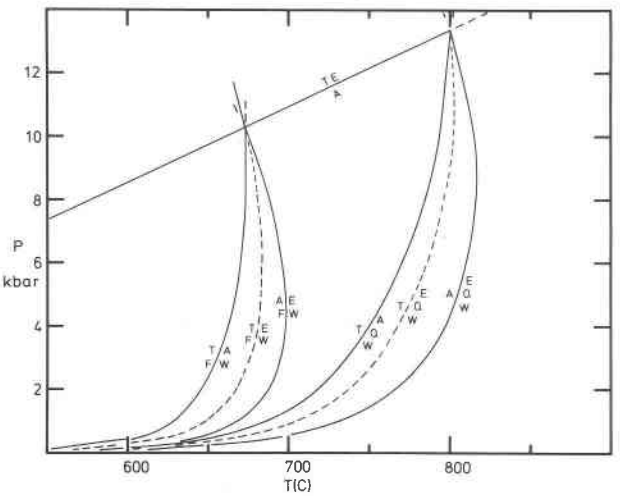

Fig. 7. Phase diagram having the maximum possible entropy of reaction AEQW.

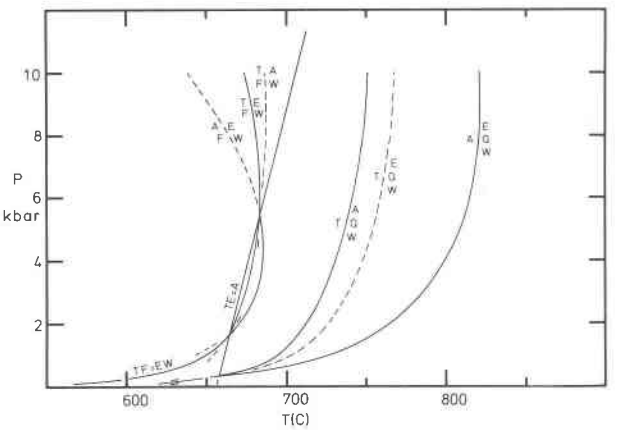

Fig. 9. Phase diagram having the maximum possible entropy of reaction TEQW.

Results

Some limiting phase diagrams

The 12 unique sets of thermodynamic data produce only seven phase diagrams that are substantially different from each other. Five sets of thermodynamic data yield phase diagrams that are topologically identical and geometrically similar to those shown in Figures 6–12. Each calculated reaction passes between or through the limiting experiments listed in Table 2.

The objective criteria used to find the sets of thermodynamic data from which the illustrated diagrams were calculated are summarized in Table 5. Also listed are objective criteria that yield the similar phase diagrams that were not illustrated and criteria that yield thermodynamic data identical to the 12 unique sets we examined. Note especially that Figure 11 was calculated from a feasible solution that may be found using any of eight different objective criteria. We have not presented the 12 unique sets of parameters we located, because these are not in any sense "best" sets of thermodynamic data but are simply 12 limiting sets from among an infinite number that might be found.

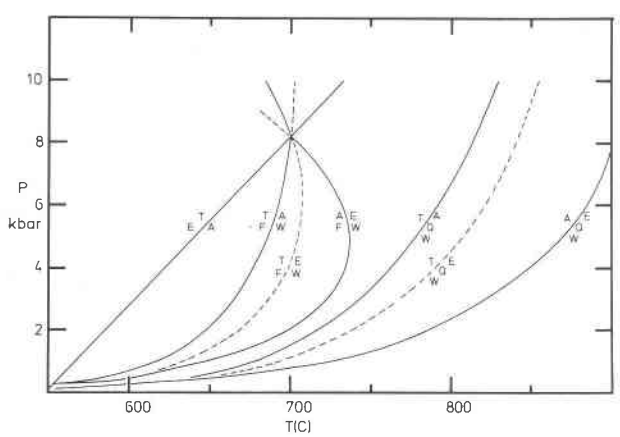

Fig. 8. Phase diagram having the minimum possible entropy of reaction TFEW.

Before discussing these diagrams in more detail, we wish to emphasize that these diagrams are nothing more nor less than possible limiting phase diagrams that are constrained only by the experiments cited and the thermodynamic assumptions in equation 2. For reasons that will be discussed below, some of these diagrams are not possible if other geological, experimental, or theoretical constraints are considered. The variation in the diagrams reflects primarily the variability permitted by the width of the experimental brackets.

The limiting diagrams differ primarily in the calculated location of reaction R7, T + E = A, relative to the dehydration reactions. Figures 6 and 7 require that the anthophyllite field terminate at high pressures. Although the calculated pressures of the invariant points (Q) and (F) are much lower, these diagrams are otherwise similar to the topology proposed by Greenwood (1963). Figures 8 and 9 are interesting because they require that invariant points (Q) and (F) each appear twice in *P–T* space. In both diagrams, invariant point (Q) appears twice in the region where calculations are possible. Invariant point (F) appears at very low pressures, in one case slightly below 100 bars, the lower limit of our ability to calculate using program TEQ. In both diagrams, in-

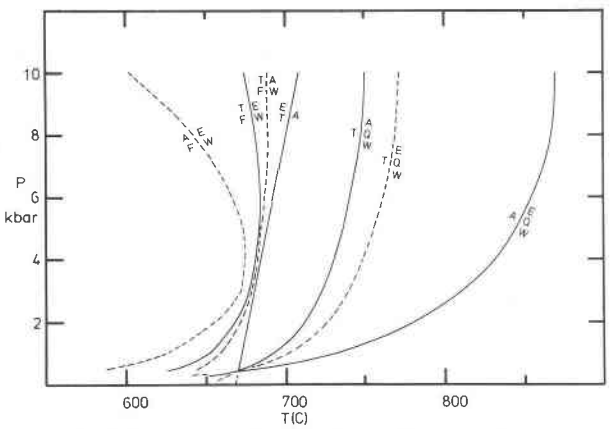

Fig. 10. Phase diagram having the maximum possible entropy of reaction TFAW.

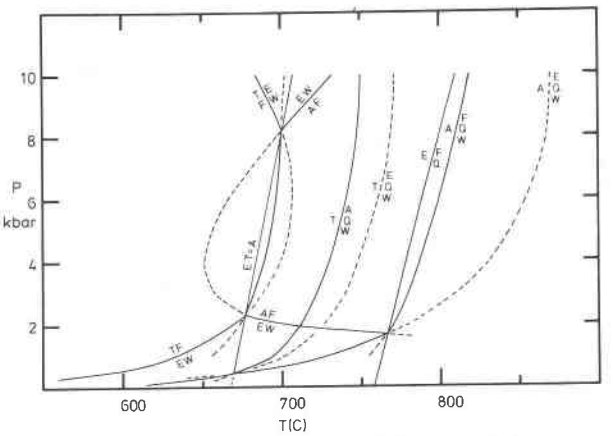

Fig. 12. Phase diagram having the minimum possible entropy of reaction AFEW.

variant point (F) must reappear at very high pressures of about 15–20 kbar, above the upper limit (10 kbar) of our ability to calculate dehydration reactions.

The upper pressure regions of Figures 8 and 9 have the topology originally proposed by Greenwood (1963), while the lower portions have the topology proposed by Hemley *et al.* (1977b). The complete topology of these diagrams was originally sketched by Greenwood (1971).

Figure 10 differs from the others because the calculated location of TEA is at higher temperatures than the other quartz-absent reactions, so that invariant point (Q) no longer appears. The quartz-absent reaction TFEW is now stable throughout its entire length, while the other quartz-absent reactions have become entirely metastable.

Figures 11 and 12 are unusual because each permits a stability field for forsterite + quartz. In all previous diagrams the stability field of this pair is restricted to temperatures higher than those illustrated. Figure 11 is similar to Figure 9 except for the complexities introduced by the presence of a low-temperature stability field for forsterite + quartz. Figure 12 differs from the other diagrams because the minimum permissible entropy for the reaction AFEW requires a reversal in the slope and curvature of this reaction. Consequently, AFEW exists as two stable segments separated by a highly curved metastable portion at intermediate pressures. This diagram would also require that enstatite become unstable above a relatively moderate temperature at all pressures in the crust.

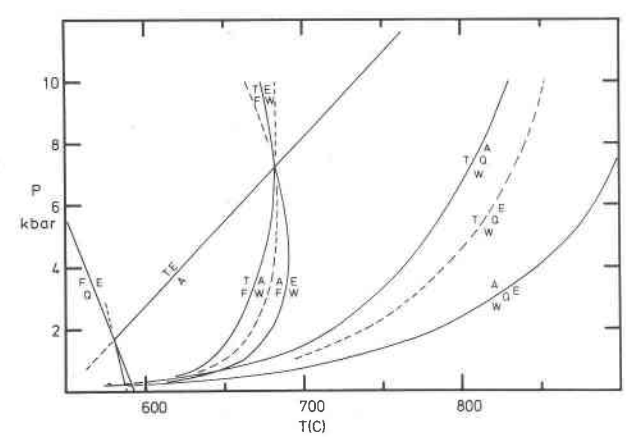

Fig. 11. Phase diagram having the minimum possible entropy of the reaction TEQW (see Table 5).

Table 5. Summary of criteria used to derive the thermodynamic data from which Figs. 6–12 were calculated. In each case, the entropy of solids in the indicated reaction was maximized or minimized. Criteria included within parentheses gave sets of thermodynamic data that were identical in every respect.

Diagram	Criteria	Criteria that yield similar diagrams
Figure 6	Min TFAW	(Max AFEW, Min TEA)
Figure 7	Max AEQW	
Figure 8	Min TFEW	
Figure 9	Max TEQW	Max TAQW
Figure 10	(Max TFAW, Max TEA)	
Figure 11	(Min TEQW, Max TFEW	
	Min AEQW, Min TAQW	
	Min TFQW, Min EFQ	
	Min AFQW, Min AFTQ)	
Figure 12	Min AFEW	Max EFQ, Max TFQW
		(Max AFQW, Max AFTQ)

Table 6. Thermodynamic coordinates of the "midpoint" of the feasible solution space and of the feasible solution in "best" agreement with calorimetric data. See text for further explanation.

	Maximum	Minimum	Midpoint	Minimum Deviation	Calorimetric Values
$H_f(Q)$	-908974	-912322	-910648	-910771	-910648 ± 1674
$S_f(Q)$	-182.364	-182.614	-182.489	-182.489	-182.489 ± 0.125
$H_f(F)$	-2168248	-2172084	-2170166	-2170166	-2170166 ± 1918
$S_f(F)$	-398.113	-399.877	-398.995	-398.995	-398.995 ± 0.882
$H_f(E)$	-1518344	-1574830	-1546587	-1544516	
$S_f(E)$	-292.818	-294.446	-293.632	-291.139	-291.139 ± 2.449
$H_f(A)$	-12061762	-12097434	-12079598	-12083059	-12083059 ± 8088
$S_f(A)$	-2447.820	-2448.054	-2447.667	-2447.750	
$H_f(T)$	-5896348	-5916790	-5906569	-5895046	-5916200 ± 7200
$S_f(T)$	-1286.267	-1286.771	-1286.519	-1273.082	-1273.082 ± 0.844

Most petrologists would agree that any diagram predicting a stability field for forsterite + quartz in the P–T range shown in our diagrams has little possible relevance for natural assemblages. On this basis alone we may eliminate Figures 11 and 12 from further consideration. Figure 12 may also be rejected by considering the experimental results of Greenwood (1963), who reversed reaction AFEW at about 700°C and 2 kbar and showed that the dehydration reaction takes place with increasing temperature. The calculated diagram predicts the wrong direction for the reaction at 2 kbar.

The rejection of these two diagrams suggests that substantial portions of the thermodynamic feasible solution space defined by the experiments we have analyzed are geologically unrealistic. Stated in another way, parts of the experimentally-bracketed temperature intervals may be geologically unrealistic. This suggestion is based on the observation that four of the twelve limiting thermodynamic data sets we found require the phase diagram topology in Figure 12 and one additional set requires the topology in Figure 11. Figure 11 may be derived (see Table 5) by taking the minimum possible slope (entropy) for the experimentally-determined reactions TEQW, TAQW, or AEQW or by taking the maximum possible slope for the reaction TFEW. The "most probable" location for these curves must therefore be nearer the maximum slopes for the first three reactions and the minimum for the last.

Figures 6–10 are very similar, and there is no obvious choice among them. The calculated locations of the reactions TFAW and AFEW differ appreciably from the experimental brackets obtained by Greenwood (1963). The most significant disagreement seems to be in Figure 6, where the calculated location of TFAW differs from Greenwood's bracket (680°C, 2 kbar) by about 100°C. Using an "anthophyllite" that differs from that used by Greenwood (1963), Nguyen Trung *et al.* (1977) have calculated thermodynamic parameters from experimental data and have estimated that the reaction TFAW occurs at 560°C, 1 kbar and at 610°C, 3 kbar (no uncertainties cited). These values are much closer to those calculated from the experiments analyzed in this study.

The problem of a "best" phase diagram

Figures 6–12 represent an analysis of the uncertainties in thermodynamic data permitted by the experimental data that is conveniently displayed by showing the permissible variation in phase diagrams. These diagrams have been calculated using the thermodynamic coordinates of some of the extreme corner points of the feasible solution space defined by the experiments. It is clear that the "best solution" from an experimental point of view is not a diagram that lies at the extreme limits of the uncertainty interval. We might argue that the phase diagram best describing the materials used in the experiments should be one that passes through the "center" of the experimental brackets corresponding to a point in the "center" of the feasible solution space.

In order to examine the problem of finding a "center" of a multi-dimensional feasible solution space, we first redefined the feasible solution space in terms of the thermodynamic properties of the individual minerals by adding constraints having the form:

$$\Delta H(\text{TEQW}) + H_f(\text{T}) - 2H_f(\text{E}) - H_f(\text{Q}) = 0$$

Substitution constraints of this form simply substitute the properties of the phases for the property of the reaction. The properties of only three phases may be derived independently because there are only three independent reactions in Table 2. Since the properties of quartz and forsterite are probably the best known and least controversial, we added the two standard error uncertainties of the entropies and enthalpies of these minerals to the set of constraints provided by the experiments. The feasible solution space defined by the experiments (Table 4), the equations of linear dependence (Table 2), and the properties of quartz and forsterite were analyzed, as described below, in order to find a "center" of the feasible solution space.

Starting at the top of the list of mineral properties

in Table 6, we performed sequentially a series of 20 linear programming computations in which we found the maximum and minimum value of a variable. The midpoint of the range was *fixed* as a constraint on the possible values of the parameter to be determined next in the list. Because this procedure clearly is not a unique definition of a "center" and because the "center" located in this manner must depend on the sequence in which the midpoints are determined, we arranged the computations so that the best known or least controversial minerals were determined first and the more problematical minerals later. Since the uncertainties of quartz and forsterite were included as constraints, the results in Table 6 show that the experiments permit the parameters to reach the maximum and minimum values allowed by the calorimetric constraints.

The derived thermodynamic parameters agree fairly well with the calorimetric data, with the exception of the entropy of talc. The entropy of orthoenstatite derived agrees fairly well with the calorimetric entropy of clinoenstatite, considering that the estimated uncertainty is simply a guess to allow for differences in the polymorphs. The enthalpy of talc derived is about three standard errors from the calorimetric value, but the entropy differs by 32 standard errors! The phase diagram calculated from the midpoint data set is shown in Figure 13.

Although Figure 13 may represent a "best estimate" for the phase diagram, in the sense that it passes through the "middle" of the experimental brackets, the thermodynamic consequences implied by this choice are severe. Although we cannot rule out the possibility that major differences exist between the talc used in the experiments and the talc used to determine the low-temperature entropy, a solution in better agreement with the calorimetric data is clearly desirable.

Thermochemical parameters measured by standard calorimetric means are available for several of the minerals considered here (Table 2), and complete agreement between these data and the parameters derived from the experiments would be very satisfying. In order to entertain this possibility, we added the two standard error uncertainty limits of all the enthalpies and entropies in Table 2 to the set of constraints provided by the experiments. We were unable to find a feasible solution for this revised problem. That is, no choice of the thermodynamic variables, within their stated two-standard-error uncertainties, satisfies the experimental data. This must

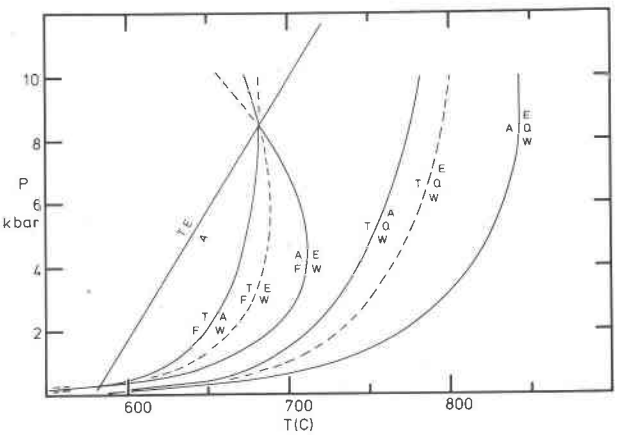

Fig. 13. Phase diagram calculated from the "midpoint" of the feasible solution space defined by the experiments in Table 4 and the calorimetric limits on the properties of quartz and forsterite (see Table 6).

be true regardless of the enthalpies or entropies assumed for those parameters that have not actually been measured.

It is not possible to determine uniquely which mineral or minerals might be the cause of this discrepancy, but our results suggest that talc is a good possibility. When the determined properties of talc (Table 1) are removed from the constraint set, feasible solutions are possible. The removal of any other single phase does not permit feasible solutions. We examined the experimental data of Greenwood (1963) in the same way and were led to the same conclusion. When the properties of talc are included in the constraints, no feasible solutions are possible, and when they are removed feasible solutions are found.

Day and Kumin (1979) have discussed an objective criterion that is useful for finding a feasible solution that is in close agreement with the available calorimetric data but which remains consistent with all the experimental data. The objective criterion (where Z is the objective function) is:

$$\text{minimize } Z = \sum_i \left| \frac{X_i - X_i'}{UX_i'} \right|$$

where X_i' is a calorimetrically-determined enthalpy or entropy of mineral i, UX_i' is the uncertainty associated with the measured value, and X_i is a value of enthalpy or entropy of mineral i that is consistent with the experiments (*i.e.* that lies within the feasible solution space). The sum is taken over all available calorimetrically-determined enthalpies and entropies, so that Z is a measure of the total deviation between a feasible solution and the calorimetric data. The op-

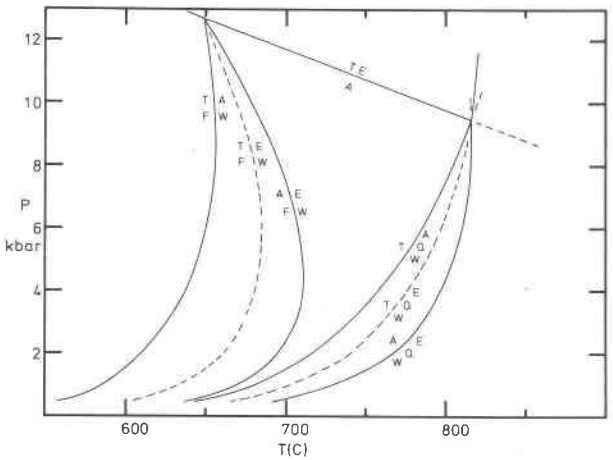

Fig. 14. Phase diagram calculated from the thermodynamic data (Table 6) that has the "minimum deviation" from the calorimetric data set that is permitted by the experiments in Table 4.

timal feasible solution is considered to be the one having the smallest possible value of the total deviation.

We have applied this criterion to the feasible solution space defined by the experiments. The enthalpies and entropies that minimize the total deviation are listed in Table 6. The phase diagram calculated using these data is shown in Figure 14. The most interesting feature of this set of derived data is that all of the calorimetric data with the exception of the enthalpy of talc are consistent with the experimental data. Virtually all the difference between the feasible solution and the calorimetric data has been assigned to the enthalpy of talc, and this is equivalent to about six standard errors in the measured value. Although other distributions of the deviations among the minerals that might not require such a large deviation for talc are possible, this may occur only at the expense of increasing the total difference. The solution reached by this procedure is a thermodynamic best fit in the sense that the sum of deviations is minimized.

Comparison with other sets of experimental data

Unfortunately, and for different reasons, it is not possible to analyze the experiments of Greenwood (1963) and Hemley *et al.* (1977a,b) together with the experiments in Table 4.

Greenwood (1963) obtained one or more brackets on each of the first six reactions listed in Table 2. Comparison of his brackets, expanded as described earlier, with the experiments in Table 4 suggests that no brackets are incompatible. The brackets for reactions AEQW and TFEW would be incompatible or nearly so if the unexpanded brackets were considered. This suggests that a feasible solution space might exist that satisfies both sets of experimental data. We combined 26 experiments from Greenwood (1963) with the constraints of Table 4, and were unable to find feasible solutions, which suggests that the two sets of data are truly incompatible. Our results do not indicate how serious this disagreement is.

Greenwood's experiments and the eight pairs of linear dependence equations are not sufficient to describe a completely-bounded feasible solution space. Consequently it is not possible to explore the boundaries of the feasible solution space in a way that will permit us to define limiting phase diagrams. A wide variety of phase diagrams would be permitted by Greenwood's experiments, but it is clear that the topology of the diagram he presented (Fig. 1) is compatible with those calculated from the experiments in Table 4. In addition, we performed a calculation to find the thermodynamic data set that satisfies Greenwood's experiments and the thermodynamic constraints on quartz and forsterite, and that also minimizes the total deviations from the calorimetric data as previously described. The phase diagram calculated from these data has a topology similar to Figure 9, in which invariant point (Q) occurs at 705°C, 6.4 kbar and at 662°C, 1.1 kbar and invariant point (F) at 657°C, 0.5 kbar and at $T < 850$°C, $P > 10$ kbar.

It is also not meaningful to treat the experiments of Hemley *et al.* (1977b) in the way we have done here, but for somewhat different reasons. The first is that their experiments are isobaric. In order to define a thermodynamic feasible solution space or to calculate a polybaric phase diagram *independent of additional thermodynamic assumptions*, polybaric data are required. The second reason is based on the way the authors interpreted their experiments. They performed experiments to determine the location, in isobaric log m(SiO_2) *vs.* $1/T$ diagrams, of reactions such as: $2T + 8H_2O = 3F + 5H_4SiO_4$. The temperature at which two or more reactions intersect is the equilibrium temperature of an orthosilicate-free dehydration reaction such as those we have studied. Hemley *et al.* (1977b) have determined preferred temperatures for these intersections at 1 kbar by fitting linear least-squares regression curves to the experimentally-determined silica concentrations and temperatures for individual reactions, or by visual fits to the same data (Hemley, 1978, personal communication). The uncertainties assigned to the pre-

ferred temperature of each intersection are reasonable estimates of the location of the dehydration reaction, but they are not absolute limits in the sense required by linear programming analysis. Standard deviations derived from regression analysis are essentially confidence intervals at some specified level of probability. In addition, regression curves are not necessarily constrained to lie *between* experiments approached from opposite sides of equilibrium. The uncertainties associated with intersections of curves fit by visual inspection may also not be absolute limits. For these reasons, it is not possible to examine the maximum range of phase diagrams permitted by the experiments in a straightforward way.

The preferred temperatures and associated errors reported by Hemley *et al.* (1977b) give estimates of the locations of the equilibrium curves that for the most part appear to be compatible with the experiments in Table 4. In order to compare their results with those obtained here, we have extended their calculated phase diagram to 10 kbar, using our programs and their preferred thermodynamic data (Hemley *et al.*, 1977b, Table 3) (see Fig. 15).

Most of the differences between their diagram and Figure 15 can be attributed to small differences in calculation procedures, but our location of AEQW, calculated using their thermodynamic data, differs significantly from their calculated position. In spite of this difference, which we are unable to explain, it is clear that their data predict a topology that agrees with the "mid-point" of the "Chernosky" data set in Table 4.

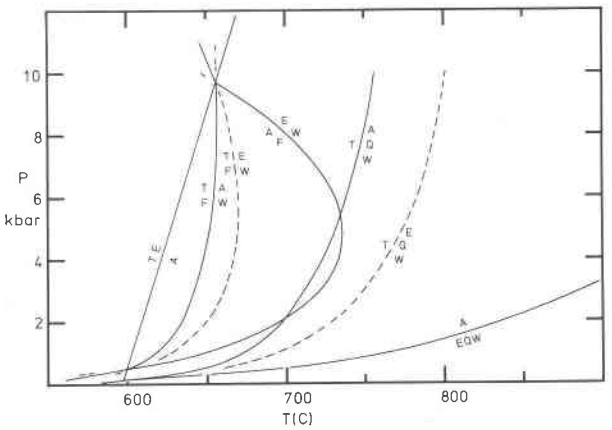

Fig. 15. Phase diagram calculated using the thermodynamic data preferred by Hemley *et al.* (1977b).

Discussion and conclusion

Figure 13 may be described as a good summary of the experimental data analyzed, because it has been derived in such a way that the calculated reactions pass through the "middle" of the experimental brackets. Figures 6–12 show the experimental uncertainty associated with this diagram. It should not be assumed, necessarily, that Figure 13 represents the "correct" phase diagram.

It is clear that most of the variation in Figures 6–12 is caused by large fluctuations in experimentally unconstrained curves. The truly discouraging range of phase diagrams consistent with the experimental data could be substantially reduced if there were even one experimental bracket for each stable or metastable reaction that can be determined in the laboratory. Two brackets, widely separated in pressure, for each of three independent reactions would also contribute to a further reduction in the variability.

Some of the permissible variation may be eliminated if thermodynamic constraints are added to the problem, but often this may not be much help. Even when a full set of thermodynamic parameters is available, the feasible solution space defined by the two standard error uncertainties may permit much more variation in the phase diagrams than the feasible solutions defined by the experiments themselves. If unconstrained thermodynamic variables are present in the problem, the linear programming algorithm tends to assign as much "error" to the unconstrained variables as is necessary to reach the limits permitted by the experiments alone. Consequently, when such unconstrained parameters are present, the range of phase diagrams permitted may be nearly as large as the range permitted by the experiments alone. In general, however, the thermodynamic and experimental feasible solution spaces do not coincide exactly, and some improvement in the "error" may be found.

Figure 13 was calculated using an entropy of talc (see Table 6) that is very different from the value determined by calorimetric methods. We have no way of deciding whether there are large differences between the natural talc used in calorimetry and the synthetic talc used in Chernosky's experiments or whether there might be an error in the calorimetric measurements, but the apparent difference seems unacceptably large. The necessity for such a great difference in the two talcs would be greatly reduced if Figure 14 were accepted as a description of the experiments. This diagram is consistent with all the experiments and all the calorimetric data, except for a

difference between the derived and measured enthalpy of talc amounting to about six standard errors in the measured value. This agreement might be made even better by accepting a solution that has a higher total deviation but which distributes some of the "error" to the other derived parameters. In addition, the calorimetric enthalpy for talc may be in error by a small amount. The close agreement of the experiments using synthetic talc (Chernosky, 1976; Chernosky and Knapp, 1977) and those using natural talc (Hemley *et al.*, 1977b) suggests that this might be the case. The effects of such small shifts in thermodynamic parameters on the calculated phase diagram are impossible to predict without performing the calculations.

We have emphasized here the apparent discrepancies between the calculated and observed properties of talc. Veblen *et al.* (1977) have recently discussed the observations of new classes of silicate chain structures, with special emphasis on their evidence for extensive disorder of chain types in amphiboles. In particular, they mention their observations of synthetic anthophyllites (including those of Chernosky used as a basis for this paper) show extensive structural disorder "in some cases consisting of intimate mixtures of chains of many widths." The effect of such structural disorder on the thermodynamic and phase equilibrium interpretation of hydrothermal experiments is debatable, but cannot be ignored. Our results suggest that a detailed electron microscope investigation of natural and synthetic talc might also be in order. The uncertainties attending our ignorance of the thermodynamic effects of possible structural disorder must be added to the already large range of possibilities due to experimental and thermodynamic uncertainties.

Our results and a comparison of these results with other experimental data suggest that a phase diagram similar to Figure 14 or Figure 13 may ultimately prove to be correct. Our results show a large range of uncertainty that prohibits a definitive answer, and a direct experimental determination of the reaction T + E = A may be the only way to discriminate among all the possibilities. The difference among the permissible phase diagrams may have an important bearing on the interpretation of natural occurrences of enstatite plus talc (*e.g.* Evans and Trommsdorff, 1974).

Our results have sobering implications concerning the possibilities for estimating equilibria that have not been experimentally determined, and even, it seems, the reliable estimation of complete phase diagrams from incomplete information. It seems to us, however, that mathematical programming techniques, such as the linear programming method we have employed here, will be useful aids for identifying the range of uncertainty in a body of experimental data, for identifying agreement and disagreement among bodies of experimental and thermodynamic data, and for finding internally consistent solutions that satisfy the available thermodynamic, experimental, and geological observations in the most agreeable way. Much additional work remains in order to develop useful criteria by which such solutions may be found, but it is clear that this approach is a useful means for analyzing existing data and planning new experiments.

Acknowledgments

This work was carried out while the senior author was a guest of Professor W. Schreyer in the Institut für Mineralogie, Ruhr Universtät-Bochum, supported by a fellowship from the Alexander von Humboldt Foundation. Halbach's work has been supported by grant Ch 4616 from the Deutsche Forschungsgemeinschaft, Bad Godesburg to N. D. Chatterjee at Ruhr Universität-Bochum. This work has been partially supported by NSF grants EAR 76 23376 and EAR77-22775 to H. W. Day and H. Kumin. At various stages, this paper has benefited from the comments of D. M. Burt, N. D. Chatterjee, J. V. Chernosky, H. Greenwood, J. J. Hemley, and J. H. Stout. Their efforts are gratefully acknowledged, but clearly the final responsibility for the views expressed here rests with us.

References

Barany, R. (1963) Heats of formation of gehlenite and talc. *U. S. Bur. Mines Rep. Invest. 6251.*

Birch, F., J. F. Schairer and H. C. Spicer (1942) Handbook of Physical Constants. *Geol. Soc. Am. Spec. Pap. 36.*

Burnham, C. W., J. R. Holloway and N. F. Davis (1969) Thermodynamic properties of water to 1000°C and 10,000 bars. *Geol. Soc. Am. Spec. Pap. 32.*

Chatterjee, N. D. (1970) Synthesis and upper stability of paragonite. *Contrib. Mineral. Petrol., 27,* 244–257.

——— (1977) Thermodynamics of dehydration equilibria. In D. G. Fraser, Ed., *Thermodynamics in Geology,* p. 137–159. D. Reidel, Dordrecht, Holland.

Chernosky, J. V., Jr. (1976) The stability of anthophyllite—a reevaluation based on new experimental data. *Am. Mineral., 61,* 1145–1155.

——— and L. A. Knapp (1977) The stability of anthophyllite plus quartz. *Geol. Soc. Am. Abstracts with Programs, 9,* 927.

Day, H. W. and H. J. Kumin (1977) Internally consistent thermodynamic data. *EOS, 58,* 530.

——— and ——— (1979) Thermodynamic analysis of the aluminum silicate triple point. *Am. J. Sci.,* in press.

Evans, B. W. and V. Trommsdorff (1974) Stability of enstatite + talc, and CO_2-metasomatism of metaperidotite, Val d'Efra, Lepontine Alps. *Am. J. Sci., 274,* 274–296.

Fisher, J. A. and E-an Zen (1971) Thermochemical calculations from hydrothermal phase equilibrium data and the free energy of H_2O. *Am. J. Sci., 270,* 297–314.

Gordon, T. M. (1973) Determination of internally consistent thermodynamic data from phase equilibrium experiments. *J. Geol., 81,* 199–208.

Greenwood, H. J. (1963). The synthesis and stability of anthophyllite. *J. Petrol., 4,* 317–351.

——— (1971) Anthophyllite. Corrections and comments on its stability. *Am. J. Sci., 270,* 151–154.

Halbach, H. and N. D. Chatterjee (1978) Über die Anwendung von Optimierungs-methoden zur Bestimmung thermodynamischer Daten von Mineralen. *Fortschr. Mineral., 56,* 34–35.

Hemley, J. J., J. W. Montoya, C. L. Christ and P. B. Hostetler (1977a) Mineral equilibria in the MgO–SiO_2–H_2O system: I Talc–chysotile–forsterite–brucite stability relations. *Am. J. Sci., 277,* 322–351.

———, ———, D. R. Shaw and R. W. Luce (1977b) Mineral equilibria in the MgO–SiO_2–H_2O system: II Talc–antigorite–forsterite–anthophyllite–enstatite stability relations and some geologic implications in the system. *Am. J. Sci., 277,* 353–383.

Holloway, J. R., D. H. Eggler and N. F. Davis (1971) Analytical expression for calculating the fugacity and free energy of H_2O to 10,000 bars and 1,300°C. *Geol. Soc. Am. Bull., 82,* 2639–2642.

Kelley, K. K. (1960) Contributions to the data on theoretical metallurgy XIII. High temperature heat content heat capacity and entropy data for the elements and inorganic compounds. *U. S. Bur. Mines Bull. 584.*

Krupka, K. M., D. M. Kerrick and R. A. Robie (1977) High temperature heat capacities of dolomite, talc, and tremolite and implications to equilibrium in the siliceous dolomite system. *Geol. Soc. Am. Abstracts with Programs, 9,* 1060.

Mel'nik, Yu. P. and V. L. Onoprienko (1969) Thermodynamic properties of anthophyllite. (in Russian) In *Constitution and Properties of Minerals,* v. 3, p. 46–55. Akad. Nauk Ukr.SSR, Kiev.

Nguyen Trung, C, M. Pichavant and A. Weisbrod (1977) Domaine de stabilite et parametres thermodynamique d'une anthophyllite problematigul. *Cinquieme reunion annuelles des Sciences de la Terre, Rennes, 19-22 avril 1977,* 351.

Robie, R. A. and D. R. Waldbaum (1968) Thermodynamic properties of minerals and related substances at 298.15°K (25.0°C) and one atmosphere (1.013 bars) pressure and at higher temperatures. *U. S. Geol. Surv. Bull. 1259.*

Skippen, G. B. (1971) Experimental data for reactions in siliceous marbles. *J. Geol., 79,* 457–481.

Veblen, D. R., P. R. Buseck and C. W. Burnham (1977) Asbestiform chain silicates: New minerals and structural groups. *Science, 198,* 359–365.

Weeks, W. A. (1956) Heats of formation of metamorphic minerals in the system CaO–MgO–SiO_2–H_2O and their petrological significance. *J. Geol., 64,* 456–472.

White, W. P. (1919) Silicate specific heats. *Am. J. Sci., 47,* 1–21.

Zen, E-an (1969) Free energy of formation of pyrophyllite from hydrothermal data: values, discrepancies, and implications. *Am. Mineral., 54,* 1592–1606.

——— (1972) Gibbs free energy, enthalpy, and entropy of ten rock forming minerals: calculations, discrepancies and implications. *Am. Mineral., 57,* 524–553.

——— and J. V. Chernosky, Jr. (1976). Correlated free energy values of anthophyllite, brucite, clinochrysotile, enstatite, forsterite, quartz and talc. *Am. Mineral., 61,* 1156–1166.

Manuscript received, October 2, 1978;
accepted for publication, March 16, 1979.